The Role of Ordered Block Copolymer Morphology in the Performance of Organic/Inorganic Photovoltaic Devices

Jason A. Gratt,[1] Robert E. Cohen[2]

[1]*Department of Materials Science and Engineering and the Program in Polymer Science and Technology, Massachusetts Institute of Technology, Cambridge, Massachusetts 02139*
[2]*Department of Chemical Engineering, Massachusetts Institute of Technology, Cambridge, Massachusetts 02139*

Received 8 July 2003; accepted 31 August 2003

ABSTRACT: A triblock copolymer consisting of hole-transport, electron-transport, and nanocluster-binding moieties was used in the fabrication of photovoltaic test devices. Depending on the casting solvent used in the device fabrication process, the morphology of the block copolymer in the devices was either an ordered, perpendicular cylindrical phase or a uniformly mixed homogeneous material. The photovoltaic action spectra of these two device types revealed clearly that the charge collection efficiency was influenced favorably by the microphase separation of the ordered system. Underlying mechanisms for these observations are discussed. © 2004 Wiley Periodicals, Inc. J Appl Polym Sci 91: 3362–3368, 2004

Key words: block copolymers; photoroltaics

INTRODUCTION

Optoelectronic devices such as photovoltaic cells, photodetectors, and light-emitting diodes are used in a variety of advanced technologies. Photovoltaic cells, for example, provide power to communication satellites and spacecraft, and are used in a variety of terrestrial applications.[1,2] Photodetectors are used extensively within spectrometers and other instruments for chemical and physical analyses. The replacement of incandescent lights in traffic signals with red and green LEDs has led to significant cost savings.[3,4] Light-emitting diodes are used in flat-panel color displays for portable laptop computers.

Traditional optoelectronic devices are based upon p–n junctions made from inorganic semiconductors such as silicon and gallium arsenide.[5] In recent years, however, there has been increasing interest in organic optoelectronic devices.[6–8] These devices are typically made from electrically conducting π-conjugated polymers,[9–11] nonconjugated polymers containing dispersed chromophores and charge transport molecules,[12,13] or nonconjugated polymers functionalized with covalently attached chromophores and charge transport groups.[14,15] The potential advantages of such organic devices include low cost, relative ease of fabrication, light weight, and mechanical flexibility.

There are a variety of fabrication schemes and resulting device architectures for organic polymer-based devices. A very simple example is shown schematically in Figure 1. Here, chromophores and charge transport molecules are blended into a solution containing a polymeric binder, and the resulting mixture is spincoated onto a clear glass or plastic substrate to yield a single homogeneous organic layer approximately 100-nm thick. The substrate is precoated with a layer of indium tin oxide (ITO), a transparent conductor that serves as an anode. A thin layer of aluminum or some other metal is evaporated on top of the device and serves as the cathode. To operate the device in its light-emitting mode, an external voltage is applied across the electrodes and charge is injected into the device. Negative charges (electrons) are injected from the cathode into the organic layer, where they are accepted into low-lying (LUMO) orbitals belonging to the electron transport molecules. A typical electron transport molecule is a π-deficient aromatic ring system, which is easily reduced upon acceptance of an electron to the corresponding radical anion.[16] Positive charges (holes) are injected into the organic layer from the anode by an analogous process. A typical hole transport molecule is a π-rich aromatic ring system that easily releases an electron into a hole of the ITO valence band, leaving behind an oxidized radical cation.[14,16] The mobile positive and negative charges move toward each other across the device under the influence of the externally applied voltage, migrating from one charge transport molecule to the next via a field-assisted hopping mechanism.[16,17] Recombination, with concomitant light emission, can occur when a hole and an electron meet near the center of the device and migrate to a chromophore molecule, pro-

Correspondence to: R. E. Cohen (recohen@mit.edu).

Journal of Applied Polymer Science, Vol. 91, 3362–3368 (2004)

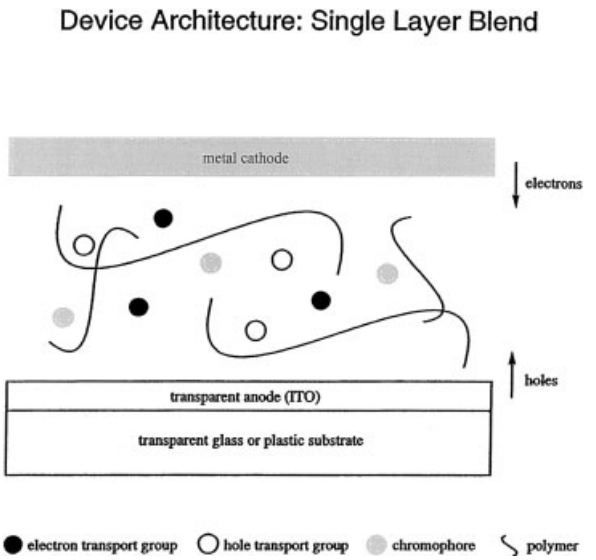

Figure 1 Schematic representation of a homogeneous blend device architecture designed for light emission.

ducing a neutral excited state that may relax back down to the ground state with emission of a bandgap-energy photon.[18] Photovoltaic activity may be obtained by irradiating the device with light such that the chromophores are stimulated to absorb photons and produce electron-hole pairs; the electrons and holes may then migrate to the appropriate charge transport molecules and drift along separate paths to the (chemically nonequivalent) electrodes, where they collect asymmetrically and produce an open circuit voltage.[19] In the single layer blend shown in Figure 1, the probability of unwanted hole-electron recombination is high because distinct pathways for each charge carrier are not provided.

The simple architecture described above is not the only one possible, and may not be optimal for all applications. The chromophores and charge transport molecules are small species that may diffuse through the polymer matrix over time and crystallize out as separate phases, leading to mechanical disruptions in the continuity of the device that ultimately result in failure during operation. Thus, it may be desirable to employ a more complex architecture in which the charge transport groups and chromophores are all present in a single layer but are covalently bound to the polymer chain, limiting their motion. A light-emitting device architecture in which the three elements (hole transport, electron transport, chromophore) are spatially segregated over appropriate length scales might be expected to minimize some of the above-mentioned problems because the majority of carriers pass through their native charge transport layer en route to the chromophore. Excess carriers thus accumulate at the chromophore interface and may eventually recombine, instead of immediately passing through the device as wasted current.[20] For photovoltaic applications, a layered or channeled architecture may facilitate the rapid separation of photogenerated carriers into spatially separate domains, leading to a reduced amount of adventitious recombination (see Fig. 2).

Block copolymers offer interesting possibilities for examining the role of device architecture on optoelectronic performance.[21,22] By varying thermal and solvent-based process histories, a block copolymer can be either kinetically locked[23,24] into a homogenized bulk morphology or it may self-assemble into any of several well-known heterogeneous morphologies. A suitably designed block copolymer with chromophores and hole transport and electron transport groups would therefore be suitable for constructing, from the same starting materials, device architectures containing either homogeneously mixed or spatially segregated components. For example, Figure 2 shows a schematic of an ordered block copolymer structure in which three distinct zones, arranged perpendicular to the device electrodes, are formed owing to the self-organization of the block copolymer.

In previous articles[25,26] we reported the synthesis and photoluminescent behavior of a diblock copolymer that contained pendant hole-transporting carbazole groups in one of the blocks. Here we extend the earlier work to a triblock copolymer that includes (a) the above-mentioned carbazole moieties, (b) a short mid-block that binds semiconductor nanocluster chro-

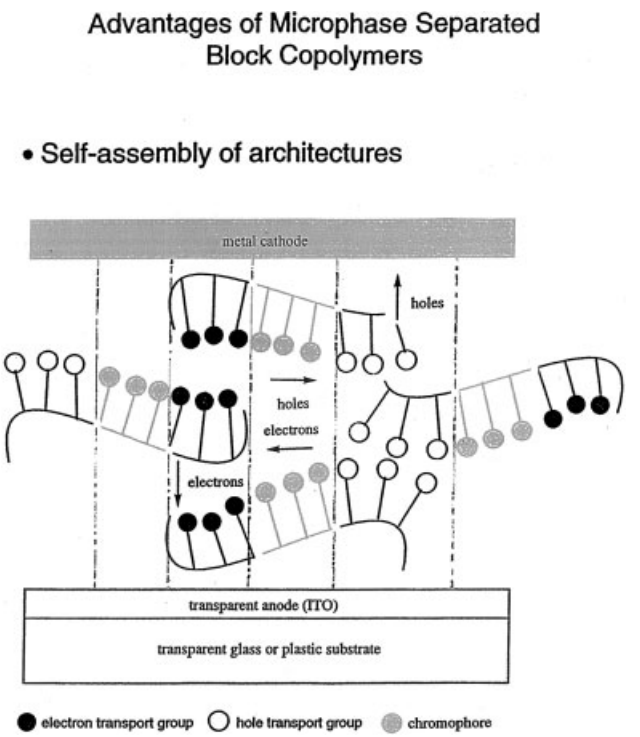

Figure 2 Schematic representation of a spatially heterogeneous architecture operating as a photovoltaic device.

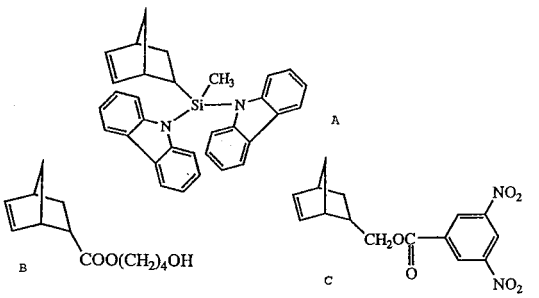

Figure 3 Repeat unit structures for the three blocks of the triblock copolymer $CAR_{200}[COO(CH_2)_4OH]_{20}DNB_{200}$.

mophores, and (c) a block that contains pendant electron-transporting groups. Through variations in the solvent-casting and annealing procedures we have been able to produce thin-film devices from this triblock copolymer in which the copolymer film is either disordered (analogous to Fig. 1) or microphase separated into a perpendicular ordered cylindrical phase (Fig. 2). These morphological differences influence the photovoltaic behavior of the devices as described in detail below.

EXPERIMENTAL

The triblock copolymer[21] used in the present study is denoted: $CAR_{200}[COO(CH_2)_4OH]_{20}$ DNB_{200}, where CAR_{200} indicates a 200 unit block of a hole-conducting carbazole-derivatized norbornene, described in previous articles.[21,25,26] DNB is a dinitrobenzene functionalized norbornene monomer[21] with good electron transport properties. The short midblock contains 20 units of a specially synthesized functionalized norbornene monomer[21] that contains ligands designed to exchange easily with $PC1Et_2$ and subsequently bind to TOPO-passivated (TOPO = trioctylphosphine oxide) CdSe nanoclusters[27] that are used as the chromophores in our photovoltaic devices. The structures of the three repeat units are shown in Figure 3.

Sequential ring-opening metathesis polymerization (ROMP) was employed in the triblock copolymerization process. The initiator, bis (tricyclohexylphosphine) benzylideneruthenium dichloride was purchased from Strem Chemical Co. Anhydrous dichlorobenzene was the solvent and ethylvinyl ether was employed in the termination step. GPC analysis (Table I) was carried out at each step of the sequential polymerization using THF as the solvent and monodisperse polystyrenes for the molecular weight standards. Further details of the polymerization and molecular characterization procedures appear elsewhere.[21,26]

Transmission electron microscopy (TEM) was performed on a JEOL 200CX instrument operating at 200 kV. Ultrathin specimens for TEM were prepared by spincoating the polymer onto a glass substrate that had been previously coated with a thin layer of BaytronP, a commercially available (Bayer Corp.), water-soluble, electrically conducting polymer. The spin-coated films were then scored with a razor blade and placed in water; the spin-coated block copolymer films floated off intact, and were collected on TEM grids for analysis of morphology.

Photovoltaic devices were fabricated by preparing 1 mL of a 1% w/v solution of the $CAR_{200}[COO(CH_2)_4OH]_{20}$ DNB_{200} triblock in the appropriate anhydrous casting solvent (chlorobenzene for microphase-separated devices; 1,2-dichloroethane for nonmicrophase-separated devices) inside a drybox. Fifteen milliliters of a $PC1Et_2$ solution in the appropriate solvent (10 mg/mL) and 5 mg of dry TOPO-coated CdSe nanoclusters (40 Å diameter) were then added, and the solution was allowed to equilibrate for 5 min. The concentrations and amounts were chosen to give one equivalent of phosphine per alcohol group and 33 wt % of nanoclusters in the final film (~10 vol %). The mole ratio of phosphine groups to nanoclusters is approximately 20 : 1.

After equilibration, the solution was taken out of the drybox and 50 μL was placed on a 1/2-inch square ITO-patterned glass substrate. A 100-nm thick film was then prepared by spinning the sample for 2 min at 1500 rpm. The ITO-patterned substrates were cleaned by etching them for 10 min in a heated ultrasonicator with 1.0 *M* HC1, rinsing them with ultrapure Milli-Q water, and degreasing them for 15 min in the ultrasonicator with a solution of 1 part Lysol cleaner and 3 parts Milli-Q water. The substrates were then subjected to three more cycles of rinsing and sonicating for 15 min each with pure Milli-Q water. After spincoating, the films were placed in a plastic storage container to protect them from dust and were allowed

TABLE 1
Gel Permeation Chromatography Analysis of the Sequential ROMP Copolymerization

Polymer	M_n (calculated)	M_n (observed)[a]	M_w/M_n
Block 1 (CAR_{200})	94,000	71,000	1.40
Blocks 1 and 2 ($CAR_{200}[COO(CH_2)_4OH]_{20}$)	98,000	78,000	1.31
Blocks 1, 2, and 3 ($CAR_{200}[COO(CH_2)_4OH]_{20}DNB_{200}$)	161,000	181,000	1.28

[a] Determined by GPC in THF using polystyrene calibration standards.

to dry overnight. Films that were annealed or pumped down under vacuum to remove traces of residual solvent did not appear to exhibit improved device performance. The cathode was then deposited by thermally evaporating a 200 nm thick layer of patterned Al lines on top of the film. Each substrate contained four testable devices formed by the square intersections of the Al and ITO lines, with an active area of 4 mm^2 each.

RESULTS AND DISCUSSION

Table I summarizes the results of GPC analysis of the products of the sequential ROMP triblock copolymerization. The calculated values of M_n are based on reactor stoichiometry, i.e., equivalents of each monomer charged relative to initiator concentration at each step of the polymerization. The observed values of M_n are not based on a universal calibration of the GPC, they represent the value of molecular weight for a polystyrene standard eluting at the observed elution time. The observed polydispersities are in the range expected for the reuthenium-based initiator. Proton NMR spectroscopy[21] of this triblock very closely resembled results obtained for a $CAR_{200}DNB_{200}$ diblock with the added presence of two very small peaks near 3.65 and 4.05 ppm. These peaks are associated with the methylene protons immediately adjacent to the hydroxyl and ester groups of the short $[COO(CH_2)_4OH]_{20}$ midblock of the triblock copolymer. The information from GPC and NMR combined with the overall high yield at each step of the sequential polymerization support the proposed stoichiometry and structure of the $CAR_{200}[COO(CH_2)_4OH]_{20}DNB_{200}$ triblock copolymer.

TEM analysis of ultrathin spincoated films was conducted using methodologies described in the Experimental section above. Spincoated films of the $CAR_{200}[COO(CH_2)_4OH]_{20}DNB_{200}$ triblock and of analogous $CAR_{200}DNB_{200}$ diblocks were morphologically featureless (i.e., not microphase separated) when 1,2-dichloroethane, a good solvent for both CAR and DNB, was employed in the process [Fig. 4(a)]. Attempts to induce microphase separation of these homogeneous films by thermal annealing *in vacuo* (21 h at 180°C) and by solvent vapor plasticization using 1,2-dichloroethane or THF were unsuccessful.

Films of the diblock and the triblock copolymers spincoated from selective solvents such as chlorobenzene, bromobenzene, and anisole showed clear evidence of a cylindrical microphase-separated morphology. The dinitrobenzene block is poorly soluble in these solvents. A 1 wt % solution of the $CAR_{200}[COO(CH_2)_4OH]_{20}DNB_{200}$ triblock in chlorobenzene forms a faintly milky colloidal solution; the DNB blocks appear to aggregate into micelles that are solubilized by the covalently attached CAR segments.

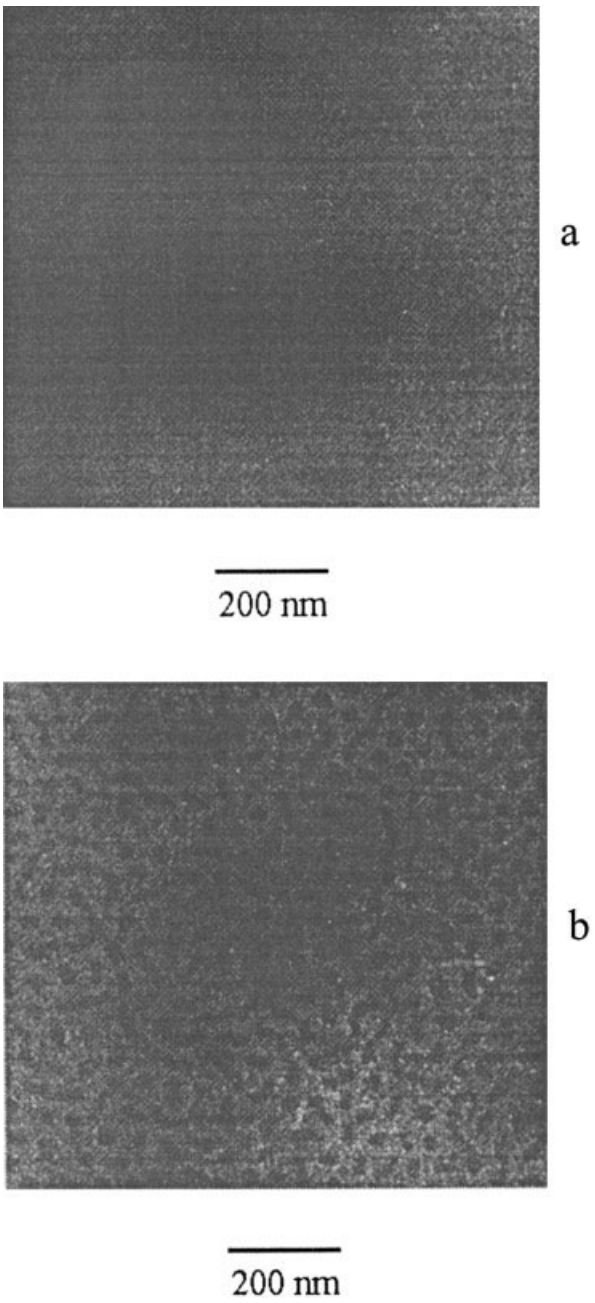

Figure 4 Plan view transmission electron micrographs of: (a, top) a homogeneous morphology cast from dichloroethane and (b, bottom) a microphase-separated morphology cast from chlorobenzene.

The polymer is thus effectively microphase separated in solution. Spincoating of the polymer appears to lay down the preexisting micelles,[28] and promotes microphase separation in the final film even though the evaporation is very rapid. Figure 4(b) shows the morphology of the triblock spincoated from chlorobenzene solution. The DNB domains are stained with $ZnEt_2$ and appear dark. The morphology is cylindrical,[21] with the long axes of many of the cylinders oriented perpendicular to the plane of the film.

Figure 4(a) and (b) indicates that we have the opportunity to produce optoelectronic devices that, depending on the solvent used in the solvent casting step of the device fabrication, contain either (1) homogeneously dispersed hole transport, electron transport, and chromophore moieties (cf Fig. 1), or (2) spatially dispersed hole transport, electron transport, and chromophore moieties (cf Fig. 2). The latter structure is particularly interesting because the periodic length scale of our block copolymer morphology is exceedingly small (ca 20 nm) and the CdSe chromophores are selectively sequestered[21] to the short cluster-binding block that resides at the cylindrical domain boundaries.

The two morphologies also offer the unusual opportunity to compare the performance of a microphase-separated device with a nonmicrophase-separated device having the exact same chemical composition. In the microphase-separated case, the DNB-filled cylinders provide continuous channels of electron-transporting material that should allow negative charges (photogenerated by CdSe clusters) to migrate efficiently through the film towards a suitable collection electrode. Because there are no hole transport groups present in these domains, the undersirable recombination with the oppositely charged carriers (mentioned in the Introduction) will be limited, increasing the collection efficiently of the device. The continuous CAR matrix surrounding the cylinders provides a similar collection path for the positively charged holes. The localization of the clusters near the domain interfaces is expected to promote rapid separation of the photogenerated charges into the appropriate regions. Devices made from nonmicrophase-separated films, in which the clusters are uniformity dispersed throughout a phase-mixed material capable of simultaneously transporting both carrier species, are expected to have a higher internal recombination rate due to the close proximity of opposite charges. The nonmicrophase-separated device should have a correspondingly lower collection efficiency.

The idea of enhancing photovoltaic collection efficiency through the use of a heterogeneous, bicontinuous structure (which may be a microphase-separated block copolymer containing hole and electron transport groups, or an interpenetrating blend of separate hole transporting and electron transporting materials) has been discussed before in the literature. Most of this work has focused on two-component systems[29,30] such as interpenetrating polymer networks, although the use of single-component systems such as microphase-separated block copolymers has received some attention.[6,22] Enhanced photovoltaic collection efficiency in C_{60}-doped MEH-PPV devices was attributed[29,30] to the formation of a bicontinuous network-like structure. No comparison was made, however, with a homogeneous (not phase separated) MEH-PPV/C_{60} blend, because such a blend was unobtainable.

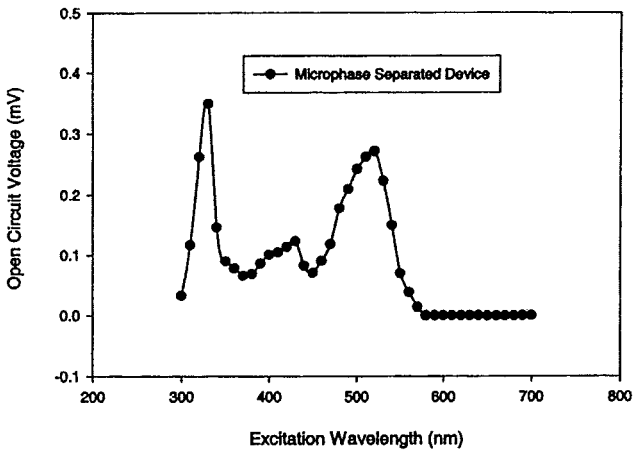

Figure 5 Photovoltaic action spectrum of the microphase-separated device.

To examine the opportunities offered by our block copolymer systems, microphase-separated and nonmicrophase-separated thin-film devices were fabricated from the CdSe cluster-loaded triblock, and the relative performances of the two types of devices were compared. The devices were prepared for testing by attaching gold wire leads to the aluminum and ITO with electrically conducting silver paint. The resistance of each device was measured with a multimeter before testing. The best devices were those that had resistances of 1 MΩ or greater. Devices with resistances of 50 kΩ or less generally gave poor results when tested, probably as a result of the presence of pinholes or electrical shorts. The devices were characterized by measuring the open circuit voltage that developed when the polymer was illuminated with monochromatic light from SPEX Fluorolog spectrophotometer equipped with a xenon lamp. The intensity of the illumination varied slightly with the wavelength, but was on the order of 2 mW/cm^2. A photovoltaic action spectrum of the open circuit voltage as a function of the excitation wavelength was obtained for each sample. Short circuit currents were generally measured at one or two specific wavelengths. The data were corrected for wavelength-dependent grating effects and variations in lamp intensity. More details appear elsewhere.[21]

Figure 5 shows the photovoltaic action spectrum of the microphase-separated device. The open circuit voltage of the device is essentially zero at excitation wavelengths longer than 600 nm, because the incident photons do not have sufficient energy to generate free charge carriers. As the excitation wavelength decreases, the nanoclusters begin to absorb light and generate electron-hole pairs. A peak corresponding to the bandgap of the clusters is therefore seen. The

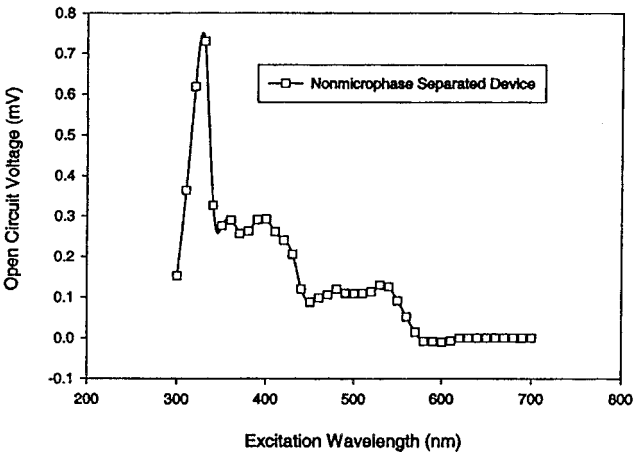

Figure 6 Photovoltaic action spectrum of the nonmicrophase-separated device.

nominal absorption maximum of 40 Å diameter CdSe clusters occurs at 550 nm, fairly close to the observed peak maximum at 520 nm. The slight blue-shift may be due to degradative effects that that decrease the effective cluster diameter, as discussed below. The polarity of the open circuit voltage is as expected, with the negative charges collecting at the lower work function ITO electrode and the positive charges collecting at the higher work function Al electrode. The magnitude of the open circuit voltage should, in principle, be upper limited by the difference in work function between the two contacts, which is approximately 0.3 eV in the case of ITO/Al.[4] The actual observed magnitude of the open circuit voltage in this sample is 0.3 mV, not 0.3 V. The low value may be a result of leakage currents in the measuring circuit as discussed in detail elsewhere.[21]

In addition to the cluster-related peak at 520 nm on the right of the spectrum in Figure 5, a peak is seen on the left side at 330 nm. This peak corresponds to the absorption maximum of the carbazole groups, which have a HOMO-LUMO gap in the near-UV and thus generate electron-hole pairs when excited at this wavelength. A third peak is seen at 430 nm. We attribute this peak to the absorption of a charge transfer complex that forms between the carbazole and dinitrobenzene groups, which similarly generates electron-hole pairs when excited.

Figure 6 shows the photovoltaic action spectrum of the nonmicrophase-separated device. A peak due to carriers photogenerated by the nanoclusters is again seen at the right at 530 nm. The intensity of this peak is very significantly lower than that of the microphase-separated device, in accord with the expectations mentioned earlier. Because the two devices contain identical volume fractions of nanoclusters of the exact same size and composition, the generation rate of carriers is likely the same in both devices at this wavelength. The lower open circuit voltage in the nonmicrophase-separated sample is thus likely to be due to the higher internal recombination rate (an effect arising from the homogenized morphology of the sample), which reduces the fraction of carriers that are successfully collected.

The charge transfer complex peak in Figure 6 at 400 nm is greatly increased in intensity in the nonmicrophase-separated sample, both relative to the cluster peak and to the corresponding peak intensely in the microphase-separated device. This enhanced intensity is a consequence of the fact that in the nonmicrophase-separated sample, the carbazole and dinitrobenzene groups are intermixed throughout the volume of the film and are favorably positioned to complex with each other. In the microphase-separated sample the groups are spatially confined to separate domains and can form complexes only at the domain interfaces.

We tested the stability of our devices by monitoring the intensity of the nanocluster peak with time for both the microphase-separated and nonmicrophase-separated devices. Table II shows the decrease in cluster peak intensity for a series of microphase-separated samples. The exact cause of the decrease is not known, but may result from the degradation of the clusters.

The degradation is most pronounced in devices that are exposed to ambient light and air, and occurs more slowly in devices that are stored inside the drybox. The cluster bandgap appears to blue-shift as the degradation proceeds. A microphase-separated device that was exposed to air for 8 days, for example, had an absorption maximum at 520 nm, shifted somewhat from the nominal absorption maximum at 550 nm, and a device that was aged for 11 days had an absorption maximum at 510 nm. The observed blue-shifts are consistent with a decrease in the effective cluster diameter, consistent with an oxidative degradation that begins at the surfaces of the clusters and works its way inwards.

CONCLUSIONS

The low current densities and limited stability of the devices fabricated in this work would restrict their use in real applications. However, important comparative

TABLE II
Degradation of Cluster Peak Intensity in Microphase-Separated Devices as a Function of Time

Time between fabrication and testing for which device was exposed to air	Ratio of cluster peak intensity to charge transfer peak intensity
8 days	2.20
11 days	0.64
15 days	0.08

information is obtained from the relative performances of the microphase-separated and nonmicrophase-separated devices. The block copolymer system developed here enabled the separate effects of morphology and composition to be deconvoluted clearly. The results clearly show that a spatially segregated structure promotes the rapid separation of photogenerated holes and electrons into spatially distinct collection networks and leads to an enhancement of photovoltaic device performance.

CMSE Shared Experimental Facilities were used in this work, and the assistance of M. Frangillo, T. McClure, and L. Shaw is gratefully acknowledged. J.A.G. thanks the Department of Defense for a graduate fellowship. J.K. Lee, W. Woo, and M. Bawendi provided helpful discussions and samples of CdSe nanoclusters. C. Leatherdale assisted in the device fabrication and photovoltaic measurements.

References

1. Markvart, T., Ed. Solar Electricity; John Wiley and Sons: New York, 1994, p. 115.
2. Sittig, M. Solar Cells for Photovoltaic Generation of Electricity: Materials, Devices and Applications; Noyes Data Corporation: Park Ridge, NJ, 1979, p. 11.
3. Ponce, F. A.; Bour, D. F. Nature 1997, 386, 351.
4. Nakamura, S. Solid State Commun 1997, 102, 237.
5. Mayer, J. W.; Lau, S. S. Electronic Materials Science for Integrated Circuits in Si and GaAs; Macmillan Publishing Company: New York, 1990, p. 82.
6. Hadziioannou, G. MRS Bull 2002, 26, 456.
7. Yang, Y. MRS Bull 1997, 22, 31.
8. Pichler, K. Philos Trans R Soc Lond A 1997, 355, 829.
9. Heeger, A. J.; Braun, D. Appl Phys Lett 1991, 58, 1982.
10. Epstein, A. J.; Blatchford, J. W.; Wang, Y. Z.; Jissen, S. W.; Gebler, D. D.; Lin, L. B.; Gustafson, T. L.; Wang, H. L.; Park, Y. W.; Swager, T. M.; MacDiarmid, A. G. Synth Metals 1996, 78, 253.
11. Onitsuka, O.; Fou, A. C.; Ferreira, M.; Hsieh, B. R.; Rubner, M. F. J Appl Phys 1996, 80, 4067.
12. Kido, J.; Shionoya, H.; Nagai, K. Appl Phys Lett 1995, 67, 2281.
13. Yamaguchi, Y.; Fujiyaam, T.; Tanaka, H.; Yokoyama, M. Chem Mater 1990, 2, 342.
14. Bellmann, E.; Shakeen, S. E.; Thayumanavan, S.; Barlow, S.; Grubbs, R. H.; Marder, S. R.; Kippelen, B.; Peyghambarian, N. Chem Mater 1998, 10, 1668.
15. Boyd, T.; Geerts, Y.; Lee, J. K.; Fogg, D. E.; Lavoie, G.; Schrock, R.; Rubner, M. F. Macromolecules, 1997, 30, 3553.
16. Stolka, M.; Yanus, J. F.; Pai, D. M. J Phys Chem 1984, 88, 4707.
17. Dabbousi, B. O.; Bawendi, M. G.; Onitsuka, O.; Rubner, M. F. Appl Phys Lett 1995, 66, 1316.
18. Tsutsui, T. MRS Bull 1997, 22, 39.
19. Greenham, N. C.; Peng, X.; Alivisatos, A. P. Phys Rev B. 1996, 54, 17628.
20. Brown, A. R.; Bradley, D. D. C.; Burroughs, J. H.; Friend, R. H.; Greenham, N. C.; Burn, L.; Holmes, A. B.; Kraft, A. Appl Phys Lett 1992, 61, 2793.
21. Gratt, J. A. Ph.D. Thesis, Massachusetts Institute of Technology; 1999.
22. di Boer, B.; Stalmach, U.; van Mutten, P.; Meltzer, C.; Kraznikov, V. V.; Hadziioannou, G. Polymer 2001, 42, 9097.
23. Cohen, R. E.; Cheng, P. L.; Douzinas, K.; Kofinas, P.; Berney, C. V. Macromolecules, 1990, 23, 324.
24. Cohen, R. E.; Bates, F. S. J Polym Sci Phys 1980, 18, 2143.
25. Gratt, J. A.; Cohen, R. E. J Appl Polym Sci 2003, 88, 177.
26. Gratt, J. A.; Cohen, R. E. Macromolecules 1997, 30, 3137.
27. Murray, C. B.; Norris, D. J.; Bawendi, M. G. J Am Chem Soc 1993, 115, 8706.
28. Boontongkong, Y; Cohen, R. E. Macromolecules 2002, 35, 3647.
29. Yu, G.; Gao, J.; Hummelen, J. C.; Wudl, F.; Heeger, A. J. Science 1995, 270, 1789.
30. Yang, C. Y.; Heeger, A. J. Synth Metals 1996, 83, 85.